Dynamical Self-assembly during Colloidal Droplet Evaporation Studied by *in situ* Small Angle X-ray Scattering

Suresh Narayanan, Jin Wang
Advanced Photon Source, Argonne National Laboratory, Argonne, IL 60439

Xiao-Min Lin
Materials Science Division, Chemistry Division and Center for Nanoscale Materials, Argonne National Laboratory, Argonne, IL 60439

(Dated: February 2, 2008)

The nucleation and growth kinetics of highly ordered nanocrystal superlattices during the evaporation of nanocrystal colloidal droplets was elucidated by *in situ* time resolved small-angle x-ray scattering. We demonstrated for the first time that evaporation kinetics can affect the dimensionality of the superlattices. The formation of two-dimensional nanocrystal superlattices at the liquid-air interface of the droplet has an exponential growth kinetics that originates from interface "crushing".

PACS numbers: 78.67.Bf, 61.46.+w, 81.16.Dn

The microscopic mechanism for self-organization of ligand-stablized nanocrystals has been well established [1, 2]. The interparticle van der Waals interaction provides the attractive force to induce the self-assembly, whereas the steric interaction due to the ligand interdigitation provides the balancing force to create stable structures. However, the macroscopic patterns created by such interactions can vary dramatically under different experimental conditions. Even for a simple case of evaporating a colloidal droplet of nanocrystals on a surface, a variety of patterns have been reported, ranging from ordered two-dimensional(2D), three-dimensional(3D) nanocrystal superlattices (NCSs) [3, 4, 5], fractal-like aggregates [6, 7] to more percolated networks [8, 9, 10]. A common notion is that the self-assembling process occurs at the liquid-substrate interface [11], where the competing effect from the diffusion of nanocrystals along the substrate and solvent dewetting could lead to pattern formation far away from equilibrium [12]. Having such vast different macroscopic structures of nanocrystal assembly hinders the exploration of their physical properties [3, 13, 14], as well as creating obstacles for device applications [11, 15]. It is therefore essential to further understand and control the nanocrystal self-assembly mechanism.

Recently, it has been shown that highly ordered 2D NCSs with domain size up to tens of microns, can be formed on a silicon nitride substrate by evaporating a nanocrystal colloidal droplet with slight excess amount of dodecanethiol ligand molecules in the solution [5]. Figure 1a shows a transmission electron microscopy (TEM) image of a region of such highly ordered NCSs. The high degree of ordering and large domain size indicates the formation of NCSs most likely occurs through nucleation and growth mechanism. It is difficult, however, to explain the high crystallinity of the superlattices through a mechanism in which self-assembly occurs on the substrate at the last instance when the solvent dewets the surface. In this letter, we report an *in situ*, non-intrusive, small angle x-ray scattering (SAXS) measurement to elucidate the formation of NCSs as the colloidal droplet evaporates. We show that, contrary to the previous notion, these highly ordered 2D superlattices are formed at the liquid-air interface of the liquid droplet during the solvent evaporation. Changing the solvent evaporation rate can lead to either 2D or 3D NCS formation using the same colloidal nanocrystals.

We used monodispersed gold nanocrystals with an average diameter of 7.5 nm and 5.8 nm in two different experimental runs [16, 17], respectively, and with the particle number concentration adjusted to be approximately $10^{13}\mathrm{mL}^{-1}$, just enough to form a monolayer. The volume concentration of thiol was 0.63%. The SAXS experiments were conducted at the 1-BM beamline of the Advanced Photon Source (APS). 10 μl of colloidal solution was deposited onto a rectangular silicon nitride substrate ($3 \times 4\mathrm{mm}^2$). The incident synchrotron x-ray beam was monochromatized to 8.0 keV by a double-crystal monochromator while two sets of horizontal (H) and vertical (V) slits were used to define the beam size to 0.2 (H) $\times$0.2 (V)mm^2. We chose a laboratory coordinate system as shown in Figure 1b so that the incident x-ray beam is along the z-direction and the substrate surface is in the y-z plane. The samples were initially aligned using the substrate as a reference, thus the top surface of the substrate was centered in the x-ray beam along the x-direction. During the experiment, the substrate was slightly titled with an angle of 0.3° relative to the incident beam. The scattered x-rays passed through a helium flight path and were collected by either an image plate (IP) or a charge-coupled device (CCD) detector.

The dynamical self-assembling process can be observed by positioning the incident beam at the bottom center of the droplet to accommodate the changing meniscus of the droplet as it evaporates. Figure 2 shows a typical time evolution of the SAXS patterns after the droplet is de-

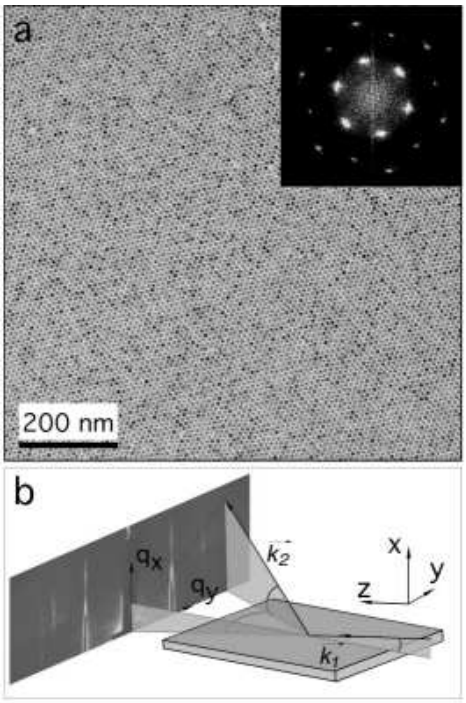

FIG. 1: Characterization of 2D nanocrystal superlattices formed by colloidal droplet evaporation: (a) Transmission electron microscopy (TEM) image of a highly ordered gold nanocrystal monolayer. Inset shows Fourier transformation of the superlattice. (b) Schematic diagram of scattering geometry used for the *in situ* SAXS measurement. The dimension of the substrate is exaggerated in order to clearly illustrate the experimental setup.

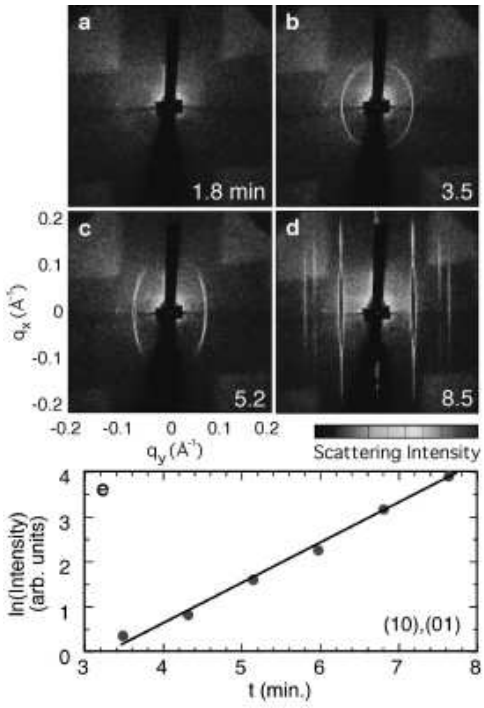

FIG. 2: (a-d)*In situ* SAXS patterns of 2D NCSs formation during the droplet evaporation. Time in unit of minute is in reference to the deposition of colloid droplet. The average diameter of the nanocrystals is 7.5 nm determined by TEM. Cross bar feature in each frame is the shadow image of the beam stop. (e) Time-evolution of the normalized scattering intensity of the monolayer powder diffraction peak for (10) powder diffraction peak (solid line is a linear fit to the data).

posited on the substrate. The droplet is evaporated in air at room temperature (23℃) with the mass of the droplet decreasing approximately at 0.66mg per minute. The initial thickness of the droplet is typically more than 2 mm. No visible scattering pattern is observed in the first two minutes indicating that, initially, there are no ordered superstructures in the droplet (Figure 2a). After that, an elliptically shaped diffraction ring is observed (Figure 2b). The section of the scattering ring near $q_y = 0$ gradually becomes more diffuse in the q_x-direction and eventually disappears, while the intensity of the scattering corresponding to the in-plane long-range order increases dramatically (Figures 2c-2d). The scattering pattern in Figure 2d remains unchanged for hours during which a thin liquid film, less than 100 μm in thickness, with a high concentration of dodecanethiol remains on the substrate surface. To illustrate the kinetics of the nanocrystal array growth, Figure 2e shows the experimental time evolution of the intensity of the (10) powder diffraction peak at $q_x = 0$, plotted in a semi-natural log format. The scattering intensity increases exponentially with time before becoming saturated after 8 minutes (data not shown). When the liquid film is completely dried and the NCSs are deposited directly on the substrate, the downward scattering is blocked by the substrate in the grazing incidence geometry [18, 19]. In contrast, the scattering patterns in the liquid film (Figure 2d) is highly symmetric in the vertical direction (q_x), indicating the 2D NCSs are formed at the liquid-air interface which is elevated above the substrate. The self-assembly of nanocrystals at the liquid-air interface was further confirmed by using a wider x-ray beam measured to be 1.5 (H)$\times$ 0.2 (V)mm^2, purposely positioned near the edge of the droplet [20]. Bragg diffraction patterns from the 2D NCSs were observed rotating along with the direct reflection of meniscus surface as the droplet flattens due to evaporation. We should emphasize that, unlike experiments carried out on the Langmuir trough [21], no aqueous subphase was used in our experiments. Both the nanocrystal ligand and the toluene solvent are hydrophobic in nature.

A comprehensive understanding of the formation of the 2D NCS monolayer, including the early stage scattering ring, can be achieved by comparing the simulated SAXS patterns during the entire evaporation process with the experimental data. The initial elliptically-shaped x-ray scattering patterns as well as its evolution can be modelled by the "powder" diffraction of 2D superlattice domains with varying x-ray incident angles. As shown in

the schematic cross section diagram in Figure 3A, the x-ray incident angle α at the liquid-air interface varies during the droplet evaporation (while the edges of the droplet are pinned at the substrate). To model the x-ray scattering patterns from the 2D lattices with their lattice plane orientation changing with time, we define a sample coordinate system (x', y') that is attached to the lattice plane as shown in Figure 3a. In a kinematical approach of x-ray diffraction [22], the averaged powder diffraction intensity from many 2D lattice domains in the reciprocal space is distributed in a circular ring defined by $\sqrt{q_{x'}^2 + q_{y'}^2} = |\mathbf{q_{h,k}}|$, where $(q_{x'}, q_{y'})$ are the momentum transfer (MT) components in the sample coordinates which satisfies the Bragg diffraction condition defined by the scattering vector $\mathbf{q_{h,k}}$. The scattering patterns recorded by the 2D detectors in the laboratory space are related to the circular powder ring in the sample space by a linear transformation between the two coordinates. Therefore the Bragg scattering condition in the laboratory coordinate is described approximately by $\sqrt{(q_x \sin\alpha)^2 + q_y^2} = |\mathbf{q_{h,k}}|$, where (q_x, q_y) are the MT components in laboratory coordinate. The short axis of the ellipse is in the q_y-direction and has a magnitude of $|\mathbf{q_{h,k}}|$, whereas the long axis is in the q_x-direction and has a magnitude of $|\mathbf{q_{h,k}}|/\sin\alpha$. For example, the elliptical scattering pattern in Figure 2b indicates, at 3.5 minutes into the evaporation process, the 2D NCSs formed at the interface which is orientated about 52.4˚ with respect to the incoming x-ray beam. The complete scattering intensity is the product of the lattice structure factor and the form factor of a spherical nanocrystal expressed as $|F(q)| = |[\frac{3(\sin(qr) - qr\cos(qr))}{(qr)^3}]|^2$, where $q = \sqrt{q_x^2 + q_y^2 + q_z^2}$ and r is the radius of the sphere. As the liquid droplet evaporates, the scattering geometry approaches a grazing incidence angle with respect to the sample ($\alpha = 0.3$˚). In this case, the scattering intensity distribution along the q_y-direction corresponds to the structure factor of the in-plane lattice and that along q_x reveals the form factor of the individual nanocrystal. Figures 3b-e show the simulation results at different stages of evaporation, based on a 2D hexagonal close-packed monolayer of nanocrystals with an average diameter of 7.5 nm (polydispersity of 7%) and a 10.3 nm center-to-center spacing. Because the incident angle can be deduced from the simulation, it is possible to obtain the NCS scattering intensity normalized by the x-ray beam footprint size. This allows a precise determination of the self-assembly kinetics. The x-ray scattering intensity data shown in Figure 2e is found to be proportional to the integrated intensity after being normalized by the changing x-ray footprint size on the sample due to the variation of x-ray incident angle.

The formation of the 2D NCSs can be understood using a kinetic "crushing" model proposed by Nguyen and Witten [23]. The diffusion constant (D) of the nanocrystals

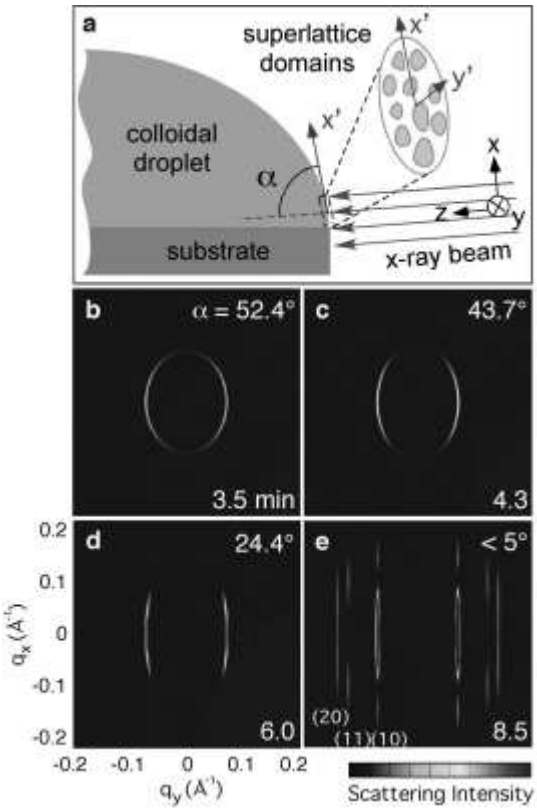

FIG. 3: Simulation results of the SAXS experiments. (a) Schematic cross sectional diagram of the x-ray beam and the colloidal droplet. (b)-(e) Simulation results based on a monolayer of 2D domains oriented at an angle α with respect to the incident x-ray beam at the liquid-air interface. The time in each frame corresponds to the real time used in our experiments.

with a hydrodynamic radius R (5.1 nm) can be estimated using the Stokes-Einstein relation ($D = k_B T/6\pi\eta R$) and the viscosity of dodecanethiol ($\eta = 2.98cp$), assuming that toluene completely evaporates near the liquid-air interface. Since the major change in scattering patterns in Figure 2 occurs at a time scale of one minute, we can compare the diffusion distance of nanocrystals in one minute with the change of liquid-air interface during the same time interval. Performing a random walk, the average distance a nanocrystal can diffuse within one minute is $\sqrt{< r^2 >} = \sqrt{6Dt} \approx 70\mu m$. Since the air-liquid interface decreases faster than 70 μm/min during the initial evaporation, as measured by monitoring the thickness change of the droplet in real-time, nanocrystals will accumulate at the 2D liquid-air interface and eventually induce 2D crystallization.

The exponential increase of the scattering intensity (Figure 2e) also supports the interface "crushing" model, in contrast to the power law behavior in the conventional 2D diffusion coarsening mechanism [24]. In the "crushing" case, the domain growth mainly occur through incorporating nanocrystals impinging the domain surface

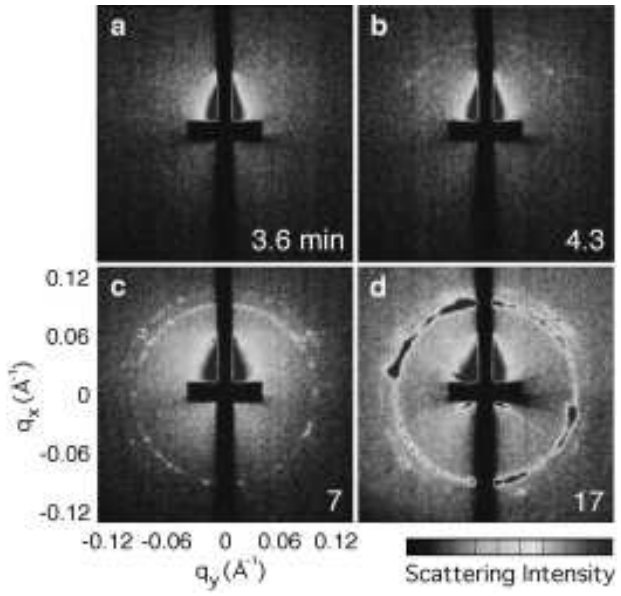

FIG. 4: In situ scattering patterns obtained during a slow evaporation of the colloid droplet. In this experiment, the average diameter of nanocrystals is 5.8 nm determined by TEM. These patterns were recorded by the CCD detector.

from below when it collapses with the evaporating liquid-air interface. The collected nanocrystals either fill the vacant sites or move to the edge of the domain. The growth rate of a domain with size S is dS/dt$\sim nSv$, where n is density of nanocrystal and v is the collapsing rate of interface. We note approximately n and v remains constant during most of the evaporation process. The "crushing" effect thus leads to an exponential growth of domain size, which is a much more dominant process than the power-law growth by 2D diffusion at the interface.

One prediction of this kinetic "crushing" model is that the formation of the 2D NCSs should be affected by the initial evaporation rate. A slower initial evaporation rate could allow the nanocrystals to diffuse away from the interface before the nanocrystal concentration reaches its critical value for 2D crystallization. The formation of superlattices will then occur in the bulk of the droplet once the overall concentration of nanocrystals in the droplet exceeds a critical concentration for 3D nucleation. Figure 4 shows the time evolution of scattering patterns when the droplet is evaporated at approximately 0.22mg per minute, much slower than the ambient condition. Indeed, 3D superlattices form and persist during the entire evaporation process. Using the same colloidal solution, but through varying the evaporation rate, both the 2D NCSs and 3D NCSs formation can be reproduced consistently.

Our measurements suggest the kinetics of evaporation can strongly affect the structure of NCS formation. 2D NCSs can form exponentially at the liquid-air interface when the evaporation is fast enough to induce nanocrystal accumulation at the liquid-air interface, whereas under a much slower evaporation condition, nanocrystals can diffuse away from the interface and 3D NCSs can eventually form inside the droplet. The kinetics driven self-assembly process observed in our nanocrystal colloidal system, might also play an important role in other complex systems. Exploring these systems using real-time x-ray scattering techniques should enable us to better control the organization of nanoscale building blocks, and also study many interesting phenomena, such as particle and domain dynamics and order-to-disorder phase transition.

We thank T. T. Nguyen, T. A. Witten, T. P. Bigioni, H. M. Jaeger and C. M. Sorensen for extensive discussions. This work was supported by the U.S. Department of Energy (DOE), BES-Materials Sciences, under Contract #W-31-109-ENG-38, by DOE Center for Nanoscale Materials, and by the University of Chicago - Argonne National Laboratory Consortium for Nanoscience Research (CNR). The use of APS is supported by Office of Science of DOE.

[1] P.C. Ohara et al., *Phys. Rev. Lett.*, **75**, 3466 (1995).
[2] Z.L. Wang et al., *J. Phys. Chem. B*, **102**, 3068 (1998).
[3] C.B. Murray, C.R. Kagan, M.G. Bawendi, *Science*, **270**, 1335 (1995).
[4] L. Motte et al., *J. Phys. Chem. B*,**101**, 138 (1997).
[5] X.M. Lin et al., *J. Phys. Chem. B.*, **105**, 3353 (2001).
[6] G. Ge, L. Brus, *J. Phys. Chem. B*, **104**, 9573 (2000).
[7] J. Tang, G. Ge, L.E. Brus, *J. Phys. Chem, B*, **106**, 5653 (2002).
[8] C. Stowell, B.A. Korgel, *Nano. Lett.*, **1**, 595 (2001).
[9] M. Maillard et al., *J. Phys. Chem. B* **104**, 11871 (2000).
[10] P. Moriarty, M.D.R. Taylor, M. Brust, *Phys. Rev. Lett.*, **89**, 248303 (2002).
[11] C.B. Murray et al., *IBM J. Res. Dev.* **45**, 47 (2001).
[12] E. Rabani et al., *Science* **426**, 271 (2003).
[13] F. Remacle et al., *J. Phys. Chem. B.*, **102**, 7727 (1998).
[14] R.Parthasarathy, X.M. Lin, H.M. Jaeger, *Phys. Rev. Lett.*, **87**, 186807 (2001).
[15] D. Weller, A. Moser, *IEEE Trans. Mag.*, **35**, 4423 (1999).
[16] X.M. Lin, C.M. Sorensen, K.J. Klabunde, *J. Nanoparticle Res.* **2**, 157 (2000).
[17] S. Stoeva et al., *J. Am. Chem. Soc.* **124**, 2305 (2002).
[18] H. Dosch, *Critical Phenomena at Surfaces and Interfaces: Evanescent X-ray and Neutron Scattering* (Springer-Verlag, New York, 1992).
[19] See EPAPS Document No. Movie for self-assembly process.
[20] See EPAPS Document No. *In situ* measurement using a wide x-ray beam positioned near the edge of the droplet.
[21] R.P. Sear et al., *Phys. Rev. E.*, **59**, R6255 (1999).
[22] B.E. Warren, *X-ray diffraction* (Dover Publications, New York, 1990).
[23] T.T. Nguyen, T.A. Witten, to be published.,
[24] A. Lo, R. T. Skodje, *J. Chem. Phys.* **112**, 1966 (2000).